National Defence / Défense nationale

MULTICHANNEL DOPPLER PROCESSING FOR AN EXPERIMENTAL LOW-ANGLE TRACKING SYSTEM

by

Éloi Bossé and Ross M. Turner
Surface Radar Section
Radar Division

DEFENCE RESEARCH ESTABLISHMENT OTTAWA
REPORT NO.1039

PCN
011LA15

May 1990
Ottawa

91-00293/

Multichannel Doppler Processing for an Experimental Low–Angle Tracking System

by

Eloi Bossé and Ross M. Turner

ABSTRACT

In this report, we present an analysis of the performance requirements for a Multichannel Doppler–Processing Unit (MDPU) which is part of the Experimental Low–Angle Tracking (ELAT) radar system. This Doppler processing unit must perform the following functions: data reduction, signal–to–noise ratio improvement, sea–clutter rejection and correction for systematic errors. Before establishing the Doppler processing requirements, we analyze the characteristics of the sea–clutter as a function of the ELAT radar parameters. Then, we present the general guidelines for the design of the MDPU, with emphasis on a new method to compensate for systematic errors. Finally, we consider the effects of block sampling on both target detection and target height estimation.

RÉSUMÉ

Nous présentons dans ce rapport une analyse de la performance requise pour une unité de traitement Doppler à canaux multiples. Cette unité de traitement doit effectuer les fonctions suivantes: réduction du nombre de données, augmentation du rapport signal sur bruit, rejet du fouillis de mer et correction des erreurs introduites par les équipements. Nous considérons les effets produits par la dimension finie de la cellule de résolution en portée en ce qui a trait à la détection et à l'estimation de la hauteur de la cible.

EXECUTIVE SUMMARY

An Experimental Low–Angle Tracking (ELAT) radar is being developed as part of a research program into high–resolution angle–estimation techniques for radar. The application of prime interest is the estimation of the height of low–flying targets such as sea–skimming missiles. Previously, radar performance has not been satisfactory against low–level threats. Reflections from the sea interfere with the desired direct–path signal and prevent an accurate estimate of target height.

The ELAT radar uses a vertical sampled–aperture antenna to test high–resolution angle–estimation techniques at sea. Because of clutter and noise, it is necessary to use a number of different processing algorithms to extract the required information for these techniques.

This report describes the design concept for a multichannel Doppler–processing unit (MDPU) which is required to perform the following functions: data reduction, coherent integration, clutter suppression, and calibration. Data reduction is required because most of the high–resolution techniques are computationally demanding and cannot produce a new estimate of height after every pulse transmission. Coherent integration is required to augment the signal–to–noise ratio (SNR). Sea clutter interferes with the proper functioning of the target height–estimation algorithms and causes erroneous detections. Therefore a filtering system is required to eliminate the clutter. Height–estimation algorithms are sensitive to calibration errors. Therefore, a system must be provided to compensate for systematic errors.

This report outlines the characteristics of the ELAT radar system and gives an analysis of the clutter problem. We present the general guidelines for the design of the MDPU with emphasis on a novel technique for compensation of systematic errors in the in–phase and quadrature receivers. We also propose a programmable array processor for implementation of the MDPU and show that an existing commercially available device can satisfy the performance requirements. Finally, we analyze how block sampling leads to a loss of samples for both target detection and target height estimation. We then show how the losses are related to the radar PRF, pulse width and target velocity.

CONTENTS

1.0	**INTRODUCTION**	1
2.0	**SEA–CLUTTER ANALYSIS**	4
	2.1 ELAT Radar Operational Scenario	5
	2.2 Sea–Clutter Model	6
	2.3 Clutter Cross Section	6
	2.4 Sea–Clutter Spectrum	8
3.0	**THE MDPU DESIGN**	13
	3.1 Doppler Processing	14
	3.1.1 Solution With One Programmable FIR Filter	15
	3.1.2 Solution Involving a Bank of Narrow Band Filters	17
	3.1.3 Results of Improvement Factor Computations	18
	3.2 Correction of Systematic Errors	23
	3.2.1 Correction of I and Q Imbalances	23
	3.2.2 Multichannel Method	26
	3.2.3 I and Q Correction in the Doppler Frequency Domain	29
	3.2.4 Experimental Verification of the I and Q Correction Technique Using a Prototype Quadrature Receiver	30
4.0	**REAL–TIME IMPLEMENTATION OF THE MDPU**	35
	4.1 Real–Time Processing Budget	35
	4.1.1 Weighting	36
	4.1.2 FFT Implementation	36
	4.1.3 Detection: Form Magnitude and Detect Largest	36
	4.1.4 Amplitude and Phase Correction for I and Q Imbalances	37
	4.1.5 Correction for the Misalignment of the Vertical Array	37
	4.1.6 Real–Time Budget Summary	37
	4.2 Proposed Implementation	38
5.0	**SAMPLING AND Doppler AMBIGUITIES IN ELAT**	39
	5.1 Sampling in the ELAT System	39
	5.2 Signal–to–Noise Ratio Analysis	42
	5.3 Velocity Ambiguities	43
	5.3.1 Doppler Visibility Region	43
	5.3.2 PRF Agility	44
6.0	**CONCLUSION**	44
7.0	**ACKNOWLEDGEMENTS**	44
8.0	**REFERENCES**	46

Multichannel Doppler Processing for an Experimental Low–Angle Tracking System

1.0 INTRODUCTION

An Experimental Low–Angle Tracking (ELAT) radar is being developed as part of a research program into high–resolution angle–estimation techniques for radar. The application of prime interest is the estimation of the height of low–flying targets such as sea–skimming missiles. Previously, radar performance has not been satisfactory against low–level threats. Reflections from the sea interfere with the desired direct–path signal and prevent an accurate estimate of target height.

New techniques such as the Coherent Height Analysis (CHA) [1] and more recently the Maximum Likelihood (ML) methods [2,3,4] show promise of solving this problem. Preliminary experimental investigations using a CW beacon on the mast of a boat to simulate a target gave very accurate results [1] even for very low targets. Radar data for higher altitude targets has been analyzed using the CHA technique with excellent results. These results were all obtained with shore–mounted vertical–array systems operating in calm sea conditions. The ELAT radar and its stabilized mount are being developed to test the CHA and ML techniques as well as other high–resolution angle–estimation techniques at sea under a variety of sea states and sea–swell conditions. Because of clutter and noise, it is necessary to use a number of different processing algorithms to extract the required information. Consequently, the ELAT radar system is composed of multiple processing units which are optimized for specific operations such as thresholding, integration, Doppler filtering, and high–resolution estimation techniques.

Since the signal processing is made up of a set of different functions coordinated to perform the complete task, a distributed approach is very attractive [5]. The distributed system is made up of the following major modules (Fig. 1):

1) The Receiver Module detects radar signals using a multichannel, sampled–aperture, receiving system. Each receiver produces analog in–phase (I) and quadrature (Q) signals via coherent quadrature baseband detectors.

2) The High–Speed Data–Acquisition Module simultaneously digitizes the sampled–aperture radar signals (I and Q) at the video rate from all channels.

3) The Signal–Preprocessing Module comprises two units. The first one is the TART unit, (TArget detection and Range Tracking) which carries out target acquisition by means of Doppler processing on the beamformed output. The second unit, the subject of this report, is the Multichannel Doppler–Processing Unit (MDPU). It provides Doppler processing for each receiver channel of the eight–element array. The MDPU only operates on the range cell containing a target detected by the TART unit.

4) The Distribution–Network Module collects data and status from various sources and distributes these signals to multiple destinations.

5) The Signal–Postprocessing Module carries out the high–resolution angle–estimation algorithms and provides graphical representation and data storage for further off–line analysis.

6) The Ship–Motion Module provides the necessary ship–motion information required for the high–resolution algorithms.

7) The Environmental–Information Module provides temperature, wind speed and direction, and sea state.

This report describes the design concept for a multichannel Doppler–processing unit (MDPU) which is required to perform the following functions: data reduction, coherent integration, clutter suppression, and calibration. Data reduction is required because the CHA algorithm is computationally demanding and cannot produce a new estimate of height after every pulse transmission. Coherent integration is required to augment the signal–to–noise ratio (SNR) in order to obtain a good estimation of height using the CHA or ML algorithms. It has been shown that coherent integration is an inherent part of ML optimal processing [4]. Sea clutter interferes with the proper functioning of the target–height estimation algorithms and causes erroneous detections. Therefore a filtering system is required to eliminate the clutter. Height–estimation algorithms are sensitive to calibration errors. Thus, a system must be provided to compensate for systematic errors.

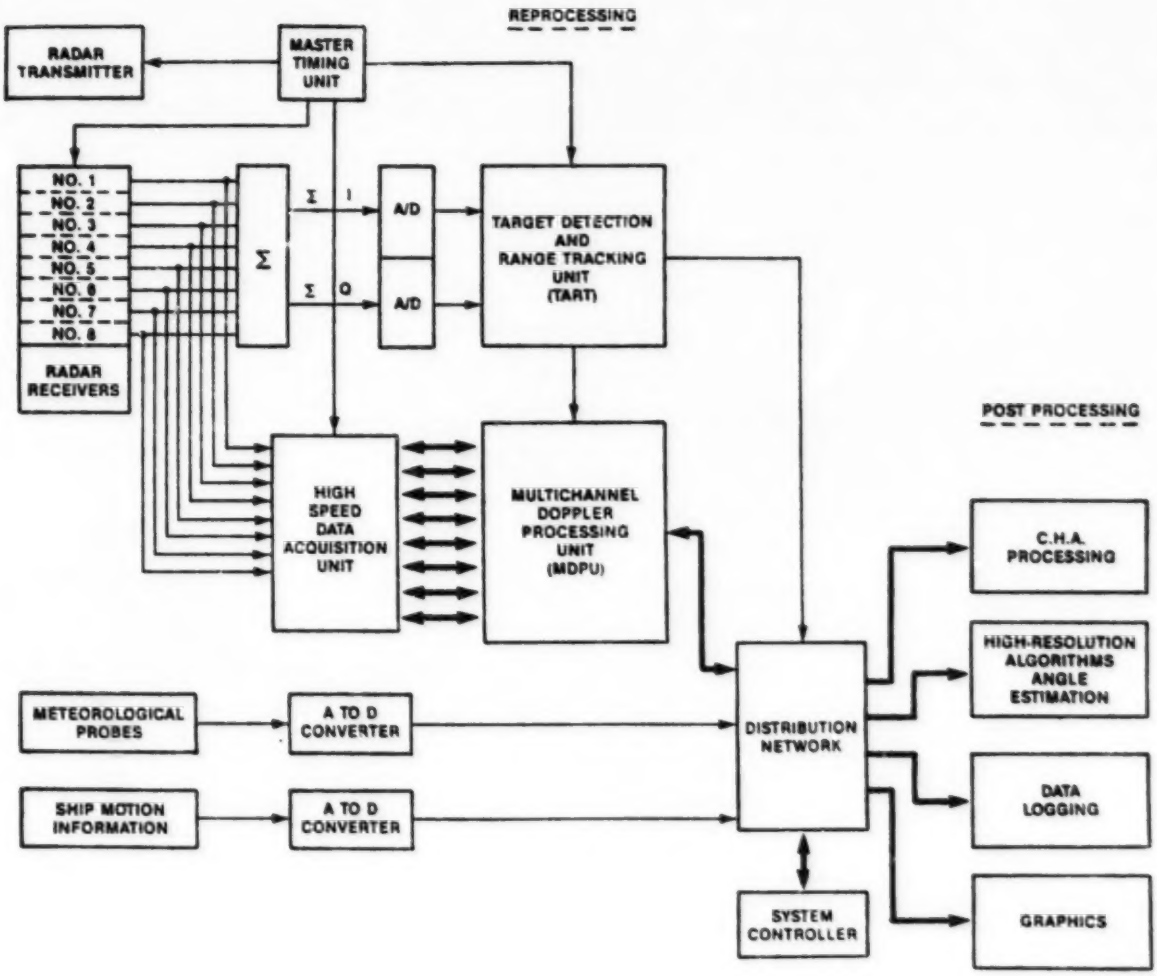

Fig.1 ELAT Signal Processing Architecture

We satisfy these requirements, except for calibration, by providing digital velocity filters or integrators for each element of the vertical–array feed. Since the target range is found using the TART subsystem [6], it is, in principle, only necessary to perform the Doppler processing on a single range cell. However, it has to be performed in parallel for each element. The system that is finally recommended is based on the FFT which covers the Doppler band with a bank of filters. This allows the Doppler resolution of the TART processor to be independent of that of the MDPU. We process data in blocks of N transmissions sampled at the selected range gate. While the MDPU is coherently integrating a block of data, the postprocessor is analyzing the results of the coherent integration of the previous block.

Section 2 of this report outlines the characteristics of the ELAT radar system and gives an analysis of the clutter problem. Section 3 presents the general guidelines for the design of the MDPU with emphasis on a novel technique for compensation of systematic errors in the in–phase and quadrature receivers. Section 4 proposes a programmable array processor for implementation of the MDPU and shows that a commercially available device can satisfy the performance requirements. Finally in section 5, we analyze how block sampling leads to a loss of samples for both target detection and target–height estimation. We then show how the losses are related to the radar PRF, pulse width and target velocity.

2.0 SEA–CLUTTER ANALYSIS

An analysis of the clutter detected by the ELAT radar is required before dealing with the clutter cancellation requirements. Sea clutter affects the operation of the ELAT radar in two ways. First, sea clutter interferes with the detection of the target and the determination of the target position. Secondly, sea clutter interferes with the accurate estimation of target height using the CHA algorithm.

The effects of sea clutter on detection have been studied in detail by numerous investigators and a significant literature exists on the subject. The effects of clutter on target–height estimation are, however, largely unknown. For the purposes of this study, it will be assumed that when the signal–to–clutter ratio, (SCR), is large enough for good detection, it is also large enough for target–height estimation. It is planned, however, to investigate the effects of sea clutter on the estimation process after clutter and multipath data have been obtained from the sea trials of the ELAT radar.

The analysis of sea clutter effects is first carried out for a "quasi–operational" scenario for two target cross sections: 1 m^2, representing a small aircraft target and 0.1 m^2, representing a generic missile target. The maximum sea state is assumed to be 5. We analyze how the ELAT radar system , with its rather low PRF's of 1KHz and 500 Hz, functions in such conditions. We then discuss the benefits of using a waveform with a higher PRF and show how certain filter types are more desirable than others for achieving the desired degree of clutter cancellation.

2.1 ELAT RADAR OPERATIONAL SCENARIO

We base our operational scenario on studies carried out by Standard Telecommunication Laboratories Ltd (STL) [7] and by Canadian Astronautics Ltd (CAL) [8]. The pertinent radar parameters are:

Operating range	: 1 km – 15 km
Target height	: 0–70 m
Transmitter type	: Magnetron
Operating frequencies	: 8.6 GHz and 9.6 GHz (X–band)
Target cross sections	: 1.0 m^2 and 0.1 m^2
Platform height	: 10 m
TX azimuth beamwidth	: 2.4 degrees
TX elevation beamwidth	: 5.7 degrees
TX gain	: 35 dB
RX gain	: 15 dB (single element)
"	: 24 dB (8 elements)
PRF	: 0.5K, 1K, 5K, 10K (Hz)
Pulse width	: 0.2, 0.5, 1.0 (μsec)
Peak power	: 65 Kw
Grazing angle	: Below 1 degree
Doppler target shift	: (1.2–12)KHz, (20–200)m/s [8.6 GHz]
"	: (1.28–12.8)KHz, (20–200)m/s [9.6 GHz]
Receiver system losses	: –26 dB

2.2 SEA–CLUTTER MODEL

We need a clutter model to determine the Doppler filtering requirements. We assume that the clutter signal is the sum of many randomly phased independent components. Applying the central limit theorem, a complex Gaussian distribution for the complex clutter signal results. We also assume a Gaussian clutter spectrum in the computation of the improvement factor. Although not completely accurate, this assumption is generally adequate, as indicated in the literature on moving–target–indicator (MTI) performance [9].

2.3 CLUTTER CROSS SECTION

In the determination of the clutter power, the amplitude of the clutter signals depends on the size of the resolution cell ($c\tau/2$) of the radar, the frequency of the radar and the reflectivity of the clutter. The clutter cross section can be expressed as:

$$\overline{\sigma} = R\ \theta_{az}\ (c\tau/2)\ \sigma^0 \tag{1}$$

σ^0 : clutter backscattering coefficient
R : range
θ_{az} : azimuth beamwidth
c : propagation speed
τ : radar pulse length

The backscattering coefficient (σ^0) is dependent upon radar frequency, sea state, grazing angle, wind and polarization. The mean value of the backscattering coefficient, σ^0, for various frequencies, sea state, grazing angle, wind and polarization are given in Nathanson [10]. Sufficient experimental data exist to recommend a conservative value of approximately –40 dB. Table 1 gives typical X–band backscattering coefficients for several sea states and grazing angles [10].

GRAZING ANGLE (degree)	0.1	0.3	1.0	3.0
SS1 Wind≈5 kts				
VV (2.66m/s)	–65	–58	–50	–45
HH	–71	–66	–51	–48
SS3 Wind≈15 kts				
VV (8 m/s)	–51	–45	–39	–38
HH	–53	–46	–39	–39
SS5 Wind≈22 kts				
VV (11.7m/s)	–44	–39	–33	–31
HH	–42	–39	–33	–32

Table 1
X–band backscattering coefficient (σ^o)dB
for several sea state conditions
and grazing angles

The clutter radar cross section is evaluated using equation (1) at the maximum design range of 15 km where the S/C ratio is a minimum. Table 2 gives the results with different transmitted pulse widths.

Pulse width (μsec)		
0.2	0.5	1.0
1.88 m^2	4.71 m^2	9.42 m^2

Table 2
Clutter Radar Cross sections
versus pulse width

With these values of clutter cross section, it is now possible to estimate the degree of clutter suppression required to achieve a given probability of detection (P_d) and false alarm (P_{fa}). The specified performance requirements are a P_{fa} of 10^{-4} and a P_d of 0.8. We assume that the clutter–residue–plus–noise has a Gaussian distribution and, therefore the Meyer plots [11] can be used. The single pulse SNR required for a Swerling type I, or II target is roughly 18 dB. We assume that the target fluctuation model is Swerling 1 so that coherent integration can be used.

A commonly used parameter to specify the clutter–cancellation capability of a processor is the improvement factor (I_F) defined as:

$$I_F = \frac{S_0/C_0}{S_I/C_I} = \frac{S_0\ C_I}{S_I\ C_0} \tag{2}$$

where

I_F	: Improvement factor
S_0/C_0	: Signal–to–clutter ratio at the output of the processor
S_I/C_I	: Signal–to–clutter ratio at the input of the processor

Converting to dB, we obtain

$$\begin{aligned} 10 \log I_F &= 10 \log (C_I/S_I) + 10 \log (S_0/C_0) \\ &= 10 \log \frac{\bar{\sigma}_{clutter}}{\bar{\sigma}_{target}} + 18 \text{ dB} \end{aligned} \tag{3}$$

With the numerical values given in this section, the improvement factors, I_F, are tabulated versus target cross section in Table 3 . We assume a P_d of at least 0.80 with a P_{fa} of 10^{-4}.

Target Cross–section	Pulse width (μsec)		
	0.2	0.5	1.0
0.1 m²	30.74 dB	34.74 dB	37.74 dB
1.0 m²	20.74 dB	24.74 dB	27.74 dB

Table 3
Improvement factor (dB) vs pulse width
and target cross section

2.4 SEA–CLUTTER SPECTRUM

The spectral distribution of the clutter is a function of various factors among which the platform motion is the most important. Internal clutter motion, system instabilities and transmitter drifts can also widen the clutter spectrum.

The radar platform motion creates two undesirable effects. The first is the shifting of the center frequency of the clutter spectrum as a function of the antenna pointing direction relative to the platform motion. The second is the broadening of the clutter spectrum resulting from platform motion normal to the antenna pointing direction. The finite beamwidth of the antenna illuminates an area on the ground or sea comprised of components each having a different Doppler velocity with respect to the radar.

The Doppler frequency (f_c) corresponding to the closing velocity between the antenna and the center of the clutter patch is given by

$$f_c = 2\,(v_s/\lambda)\cos\theta\cos\psi \tag{4a}$$

with

λ: Wavelength

v_s: Ship velocity

θ: Azimuth angle between platform velocity and the direction of the antenna beam.

ψ: Depression angle for an shipborne antenna.

The ELAT radar antenna system is mounted on a ship and operates at grazing angle, ψ, of less than one degree ($\cos\psi \approx 1$). The spectrum of the signal received by such an antenna system might appear as shown in Fig. 2. The main–lobe clutter position in the frequency domain is not fixed because of changes in ship velocity. Since the radar beam has a finite width, not all scatterers are at the same azimuth angle with respect to the direction of v_s. If the finite beamwidth of the antenna is taken as $\Delta\theta = \theta_1 - \theta_2$ in Fig.3, then the Doppler spread is:

$$\Delta f_c = 2\,(v_s/\lambda)\,(\cos\theta_1 - \cos\theta_2) \cong 2\,(v_s/\lambda)\,\Delta\theta\sin\theta \tag{4b}$$

since $\Delta\theta$ is normally small.

Bearing in mind the Gaussian assumption, the standard deviation of the Doppler spectrum due to platform motion is

$$\sigma_m \cong (v_s/\lambda)\,\Delta\theta\sin\theta \tag{5}$$

When the antenna points in the direction of the platform velocity ($\theta = 0°$), the Doppler shift f_c of the clutter is maximum but the width of the Doppler spectrum, Δf_c, due to platform motion is minimum. On the other hand, if the antenna is directed perpendicular to the direction of the platform velocity ($\theta = 90$ degrees) the clutter Doppler center frequency is zero but the spread is maximum. Assuming a maximum v_s of 8 m/s ($\cong$ 15 knots), the maximum Doppler shifts can vary from 458.6 Hz up to 512 Hz corresponding to the two RF transmission frequencies of 8.6 GHz and 9.6 GHz respectively. The method selected to suppress the clutter should be adaptive to the velocity of the ship.

A second contributor to the spectral shape of the clutter is clutter random motion. The scatterers forming the clutter return often move in the wind causing a spreading of the clutter spectrum. Because of the randomness of the motion from scatterer to scatterer, the spectral contribution is assumed to be Gaussian. The standard deviation of the clutter is related to the apparent velocity spread, Δv, of the scatterers as in [12,13]:

$$\sigma_c = 2\,\Delta v\,/\,\lambda \tag{6}$$

Furthermore, the transmitter frequency instability from pulse–to–pulse spreads the clutter spectrum [9, page 216] according to the following equation:

$$\sigma_g = 2.67\,(1/2\pi)\,(\Delta f/\Delta t)\,/\,(1/\tau) \tag{7}$$

where

σ_g: standard deviation due to transmitter frequency instability

Δf: transmitter instability in frequency

Δt: 1/PRF (interpulse period)

$1/\tau$: transmitter bandwidth (τ=pulse width).

These system instabilities contribute to the spread of the clutter spectrum. We make the assumption that the resultant function is also Gaussian with a variance that is the sum of the individual variances as

$$\sigma_d^2 = \sigma_m^2 + \sigma_c^2 + \sigma_g^2 \tag{8}$$

A NUMERICAL EXAMPLE FOR THE ELAT SYSTEM:

The computations involved in (8) are performed with a set of parameters which are typical of the ELAT system:

V_{ship}	= 8 m/s (≈15 knots)	
θ	= 90°	
ψ	= 0°	(grazing angle)
$\Delta\theta$	= 2.4°	(antenna beamwidth)
PRF	= .5, 1, 5, 10 (KHz)	
τ	= 200 nsec	(pulse width)
Δf	= 28 KHz	[17, section 17.3]
λ	= 3.125 cm	(f=9.6 GHz)
Sea state	= 3	
$\lambda\sigma_c$	= 160 cm/sec	[15, p.100]

The computations indicated in (5), (6), (7) for the platform motion, internal clutter motion and transmitter instabilities give the resultant standard deviations:

PRF			
0.5 KHz	1 KHz	5 KHz	10 KHz
Standard Deviation			
52.3 Hz	52.4 Hz	53.7 Hz	57.6 Hz

Table 4
Standard Deviation of Clutter Spectrum
vs PRF (Hz)

The above standard deviations for the sea clutter spectrum are in reasonable agreement with published data which lie in the range (60–100 Hz), for comparable sea conditions [12–15]. We will use σ_d=60 Hz in the subsequent computations.

In summary, the width of the power spectrum of the clutter (σ_d) tells us the approximate width needed in the stop band of the filter to reject the clutter (e.g.120 Hz). The velocity of the ship and other related information tell us where to tune the rejection filter with respect to the center frequency of the main–beam clutter.

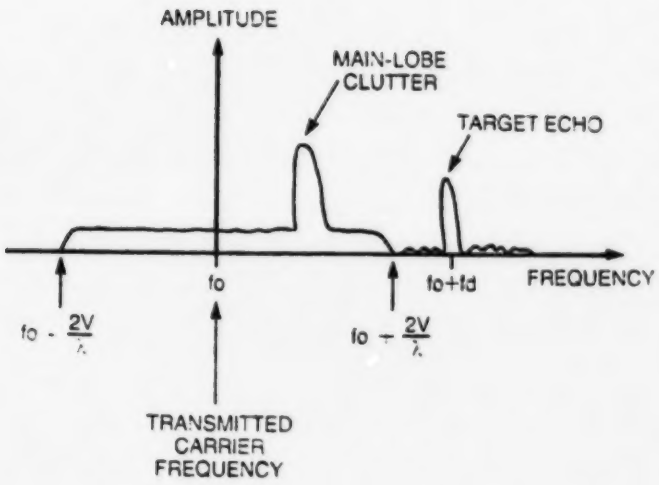

Figure 2
Spectrum with a Shipborne Radar Platform

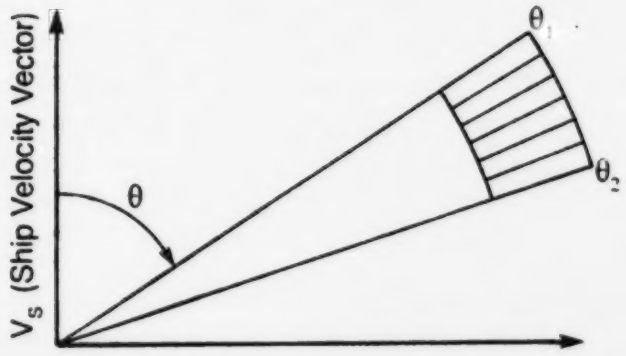

Figure 3
Effect of Ship Motion on Doppler Spread

3.0 THE MDPU DESIGN

Here we describe some solutions that satisfy the processing requirements defined in the introduction: SNR improvement, data reduction, coherent processing and clutter rejection. As mentioned in the introduction, all these functions are implemented by Doppler processing. Figure 1 shows a block diagram of the ELAT signal–processing architecture.

The radar employs separate transmit and receive antennas. The ELAT receive antenna consists of 8 linear elements illuminated by an offset parabolic cylindrical reflector. The signal received at the each element is amplified, downconverted to an intermediate frequency, and converted to baseband using quadrature video detectors that produce in–phase (real) and quadrature–phase (imaginary) video signals. The conversion to digital is performed on the beamformed output for the detection. This is done in the Target Acquisition and Range Tracking (TART) unit. Other analog–to–digital (A/D) conversions are performed in the high–speed data–acquisition module on each of the eight receivers to form the complex signal vector used in the MDPU.

The target is acquired by TART unit. The signal–processing operations in the TART unit comprise the application of Doppler filtering to the beamformed output of each range cell. This is followed by thresholding to detect the presence of a target. Here the beamforming operation is the simple addition of the I and Q outputs from each of the eight antenna feed elements which form a beam broadside to the antenna. The TART unit determines the range cell with the highest amplitude and transmits the corresponding range information to the Master Timing Unit (MTU). Thresholding and target declaration are performed in the MTU.

If a target is declared in the MTU, the range information is transferred to the high–speed data–acquisition system. This system acquires data from each of the eight receiver channels sampled at the range cell where a target has been declared. The in–phase and quadrature signals from each of the eight receivers are digitized to form eight complex signal samples which are subsequently directed to the MDPU. The MDPU has two main functions, Doppler processing and the correction of systematic errors originating from the vertical array and between the I and Q channels.

3.1 DOPPLER PROCESSING

The development of the MDPU is motivated by the requirements of the CHA algorithm as implemented on the CHA data processor, an AP–120B array processor. The CHA algorithm is computationally demanding so that this unit can only process a data vector every 20 ms (50 Hz) [16]. A data vector represents the set of antenna outputs collected at a particular instant of time (snapshot). As data vectors are received from the data–acquisition system at a 2 KHz rate (dual–frequency operation), there is an obvious need for a data reduction by a factor of at least 40. Fortunately, the optimal procedure for the CHA data processor is coherent integration of all data vectors prior to delivery to the CHA data processor [4].

Doppler filtering is a form of coherent integration that both eliminates clutter and increases the signal–to–noise ratio. However, the clutter has a Doppler spread and an offset Doppler frequency that depends on both the ship direction and the sea wave motion. It is therefore necessary to have a degree of control over the filter stop band while enhancing the signal–to–noise ratio.

Before starting the filter design, it is necessary to answer the following questions:

What is the desired resolution ?
How many data points, N, are needed?
What is the potential dynamic range of the signals?
What weighting function should be used?

The term "resolution" has both a general and a specific sense. In the general sense, resolution is defined as the ability to separate two or more spectral components and correctly identify their presence and their frequencies. However, this depends on the relative strength of the signals, the SNR and our knowledge of the response curves to each individual signal. For this reason, a more specific sense of resolution is used in signal processing. Here resolution is defined as the width of the response curve between half–power points; this is historically known as the Rayleigh criterion. Such a frequency separation is regarded as sufficient to reliably resolve two equal–strength signals. It is not, however, sufficient to resolve unequal–strength signals. The mainlobe of the weaker signal will be confused in the sidelobe response of the stronger signal. In that case, weighting is

used to reduce the filter sidelobes and the effect is to broaden the peak of the response curve thus degrading the resolution. A digital filter with an unweighted response curve has a resolution defined as f_s/N (f_s = sampling frequency).

The number of data points to be integrated depends, among other factors, on the target speed and radar range–resolution cell and corresponds to the block size. We have carried out an analysis of the effect of block sampling on target detection and height estimation in section 5. Doppler filtering is performed by integrating N successive samples from the same range cell. For the ELAT system, a block size of 64 is a reasonable compromise, although as shown in section 5, some limitation on target velocity will have to be accepted.

The dynamic range of the signals is limited by the 12–bit ADCs of the channel data–acquisition system [5]. In the ELAT system, automatic gain control is provided to maintain the signal in this dynamic range.

The choice of a weighting function determines how large the difference in amplitudes between two signals may become before the sidelobe response to the stronger signal is confused with the mainlobe response to the weaker signal. The weighting function strongly influences the degree of clutter suppression achievable. We will study the effects of choosing different weighting functions by observing how these affect the MTI improvement factor as a function of target Doppler frequency.

The following sections consider how to satisfy these requirements by using either a single FIR (Finite Impulse Response) filter or a bank of narrow–band filters.

3.1.1 SOLUTION WITH ONLY ONE PROGRAMMABLE FIR FILTER

This section derives a solution where a single or at most two programmable FIR filters are used to cover the Doppler frequency band of interest. The Doppler frequency shift of the clutter varies with the speed of the radar platform, the direction of the antenna in azimuth and the elevation angle to the clutter. Thus, the clutter rejection notch needed to cancel the clutter cannot be fixed, but must vary. The approach proposed in this sub–section is a programmable digital filter for each channel. The frequency–response curves of these filters can be shaped to account for prior knowledge of the velocity of the platform and the direction of antenna pointing.

As shown in section 2.2, it was convenient and reasonable to assume a Gaussian clutter spectrum of the form:

$$P_c(f) = (1/\sigma_d \sqrt{2\pi}) \exp\left((f-f_m)^2/(2\sigma_d^2)\right) \tag{9}$$

σ_d : as defined in (8)

f_m : Doppler shift due to relative motion between radar platform and the clutter.

To compute the improvement factor defined in (2), we use the clutter and the signal covariance matrices. Assuming stationarity, the k,ℓ^{th} element of the clutter covariance matrix, $\mathbf{M}_c$, [17] is given by

$$\mathbf{M}_c(k,\ell) = \exp\left[-2(\pi\, \sigma_d/PRF)^2(k-\ell)^2 - j\, 2\pi\, (f_m/PRF)\, (k-\ell)\right] \tag{10}$$

In the same way as above for the clutter, the k,ℓ^{th} element of the signal covariance matrix, $\mathbf{M}_s$, is given by

$$\mathbf{M}_s(k,\ell) = \exp\left[-j\, 2\pi\, (f_d/PRF)\, (k-\ell)\right] \tag{11}$$

where f_d is the target Doppler shift

The improvement factor when the input powers of both signal and clutter are normalized to unity is

$$I_F = \frac{\mathbf{w}^H\ \mathbf{M}_s\ \mathbf{w}}{\mathbf{w}^H\ \mathbf{M}_c\ \mathbf{w}} = \frac{S_0\ C_I}{S_I\ C_0} \tag{12}$$

where $\mathbf{w}^H$ is the transposed complex conjugated of the weight vector associated with the filter of interest.

The limitation of this approach is that the FIR filter can be programmed to have its passband centered on the target only if we know the target speed. In an experimental system such as ELAT, the target speed is determined during the detection and acquisition phase using the TART processor. However, it is not necessarily true that block size and hence the Doppler resolution is the same for both detection and estimation. For example,

if a coarser resolution was used for detection than for estimation, it would be necessary to cover the Doppler uncertainty window with several filters.

3.1.2 SOLUTION INVOLVING A BANK OF NARROW BAND FILTERS

Here we consider the more general approach of passing the data through a bank of narrow–band filters. Since the noise is wide–band, its energy is divided among the various filters. However each target return has its energy concentrated at one specific Doppler frequency. A bank of narrow band filters actually reduces the average value of the noise by eliminating many of its frequency components. We consider here two classes of Doppler filter bank, the weighted DFT and FIR filter banks.

The DFT filter bank comprises a set of filters that have identical characteristics except for the mainlobe position. Identical filters can be synthetized using the FFT. FFT filters represent a restricted class of FIR filters having weighting coefficients that are not optimum because they cannot be defined independently for each filter. However the FFT is a computationally efficient method to implement a bank of narrow–band filters. The computational efficiency of the FFT results from the reduction in number of multiplications since a single multiplication provides data to more than one filter output.

The FIR technique is much more flexible than the DFT technique for the design of the filter transfer function. This is because the weights for an FIR filter can be changed for different environments thus changing the sidelobe characteristics of the filter. If necessary, the FIR technique allows for filters that are non–identical in order to concentrate the low sidelobes in the frequency range of the clutter interference. Another advantage is the flexibility in processing any number of data. FFT filters for radix 2 can be implemented only for data sequences where N is a power of two. If N is not a power of two, it is sometimes efficient to expand the number of samples to the next power of two by the addition of zeros. In spite of the advantages of the FIR technique, we choose the FFT technique because it is obviously easier to implement and it can meet all of our system requirements.

The use of the DFT to synthesize a bank of narrow bank filters is constrained by the same requirements stated in the previous section for a single filter (weighting, number of samples, etc.). The scheme for mainlobe–clutter rejection in DFT is simply not to use the

DFT outputs in the vicinity of the mainbeam clutter spectrum which is correctly tracked if the ship motion is known. We recommend the weighted DFT approach using an FFT algorithm for the MDPU design. We will show that this design satisfies the system requirements while leaving flexibility for future system improvements.

3.1.3 RESULTS ON IMPROVEMENT FACTOR COMPUTATIONS

To evaluate the improvement factor (12) of the Doppler filter bank, we consider the effect of the following three factors:

1) the weighting function (vector $\mathbf{w}$);
2) the block size for integration;
3) and the PRF.

In Figure 4, we show the effects of using four different weighting functions: rectangular, Hann, Hamming and Blackman. It is clear that, in the region of the mainbeam clutter, the value of the improvement factor is roughly the same even with different weighting functions since the clutter energy suppressed by the sidelobe reduction is recovered in the widening of the filter mainlobe. On the other hand, in the target visibility region, the choice of a weighting function is important. A weighting function with a rapid sidelobe fall–off (dB/octave) is preferable. As illustrated in Figure 4, the Blackman window gives the best improvement factor in the visibility region since the clutter is more rapidly and deeply suppressed. This occurs because the Blackman window has the most rapid sidelobe fall–off (–18 dB/octave) [18]. The sidelobe fall–off rates for the Hann, Hamming and rectangular windows are respectively –12, –6 and –6 (dB/octave).

The oscillations on the curves presented in Figure 4 are due to a phenomenon called the scalloping or picket–fence effect. The scalloping effect is the observed dip in the improvement factor for a Doppler frequency lying midway between two DFT bins.

In Figure 4, we have indicated the visibility region for a target cross section of 1 m^2. The visibility region is complementary to the clutter region. It represents the region where the target can be detected. Obviously for other target cross sections the visibility region can easily be determined by moving the threshold up and down by an amount in dB which is just equal to the change in target cross section. For the parameters selected, the visibility region occupies 60% of the spectrum which is acceptable for ELAT experiments.

In Figure 5, we see the dependence of the improvement factor on the window length or block size, N. Improvement factors are plotted versus Doppler frequency normalized with respect to PRF for N = 32, 64, and 128. We note that the scalloping effect becomes more fine–structured as N increases.

Because the sidelobes for the Blackman filter fall off at a rate of –18 dB/octave, as the target Doppler moves away from the clutter region into the visible region, we observe a constant increase in the improvement factor, I_F. This is in contrast to Fig.6 where I_F is plotted versus normalized Doppler frequency for a Hamming window having sidelobes that fall off at a rate of –6 dB/octave. In Fig.6, as the Doppler frequency moves away from the clutter region into the visible region, I_F increases to a certain point and than levels off as a result of the sidelobes of the Doppler filters picking up clutter.

Finally, we observe that the improvement factors achieved with the Blackman filter in the visible region (Fig.5) are much larger than those achieved with the Hamming filter (Fig.6). As well, an increase in N gives a much larger improvement in the visible region for the Blackman filter than it does for the Hamming filter. These effects may be important when dealing with very small but fast targets.

We now consider the effect of increasing the PRF. We must be careful how we analyze these effects because there are two ways of doing it. First, suppose we increase the PRF from 1 kHz to 5 kHz. If we maintain the block size the same, say 32 samples, then at 1 kHz, the data span 32 milliseconds and the resolution is 1 kHz/32 while at a PRF of 5 kHz, the data length is 6.4 milliseconds and the resolution is 5 kHz/32. That is, by increasing the PRF we have decreased the Doppler resolution. This leads to the type of result shown in Fig.7; when the PRF changes from 5 kHz to 10 kHz we observe almost no change in the fractional Doppler visibility region but instead, an actual increase in the width of the clutter blocked region.

Now, consider the correct way of analyzing the problem. Real radar systems are almost always power limited and almost always operate at maximum power output. Therefore, if the PRF is increased, the pulse width must be decreased so as not to exceed the transmitter power limitation. Also, the time taken to search a region is set by the power–aperture product of the radar. If we don't change the power output of a radar, the dwell time to search a given direction does not change. If we compare performance on the

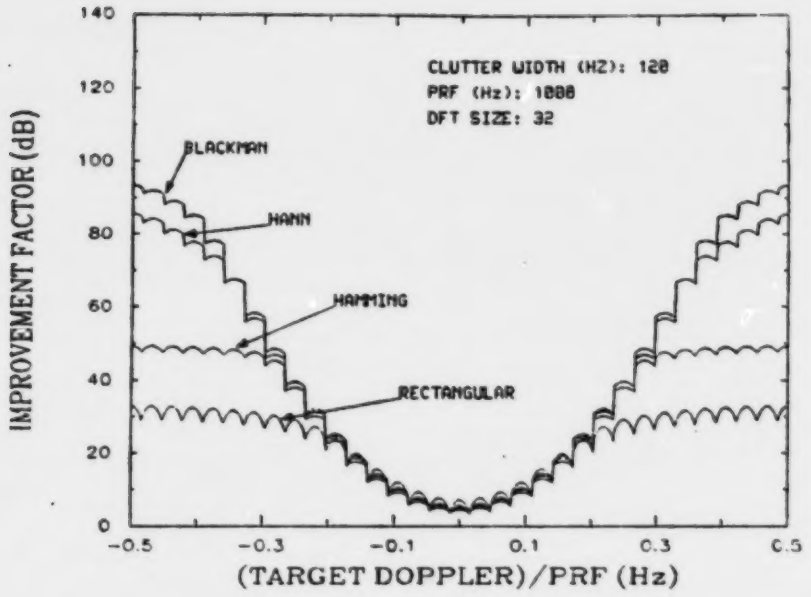

Figure 4:
The Effect of Weighting Functions on the Improvement Factor

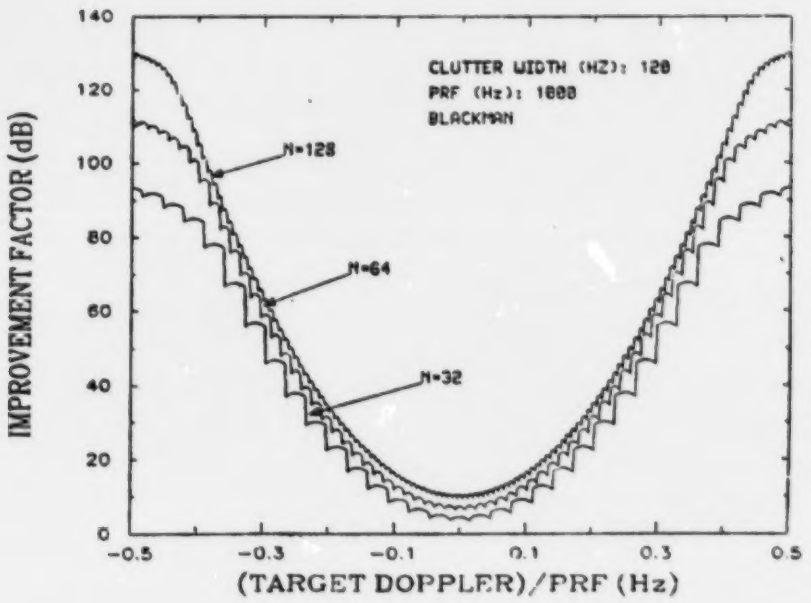

Figure 5: The Effect of Window Length (Blackman)

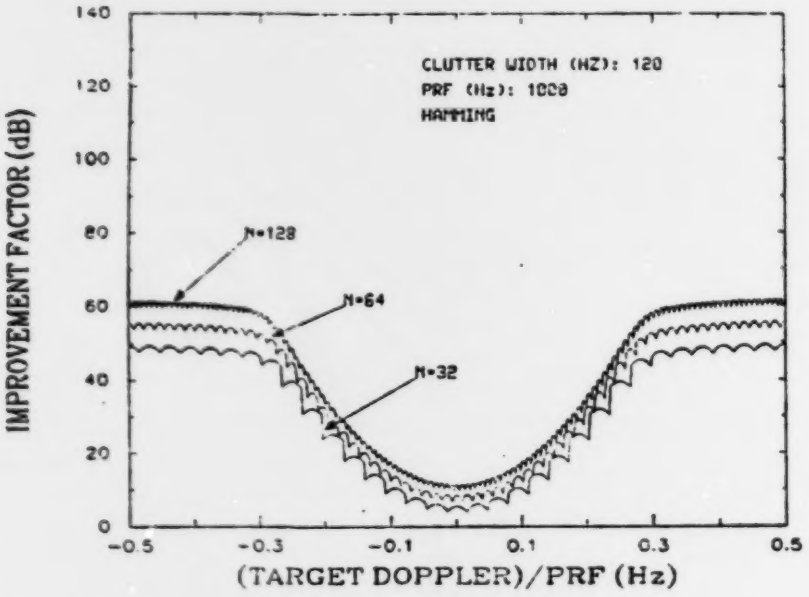

Figure 6
The Effect of Window Length (Hamming)

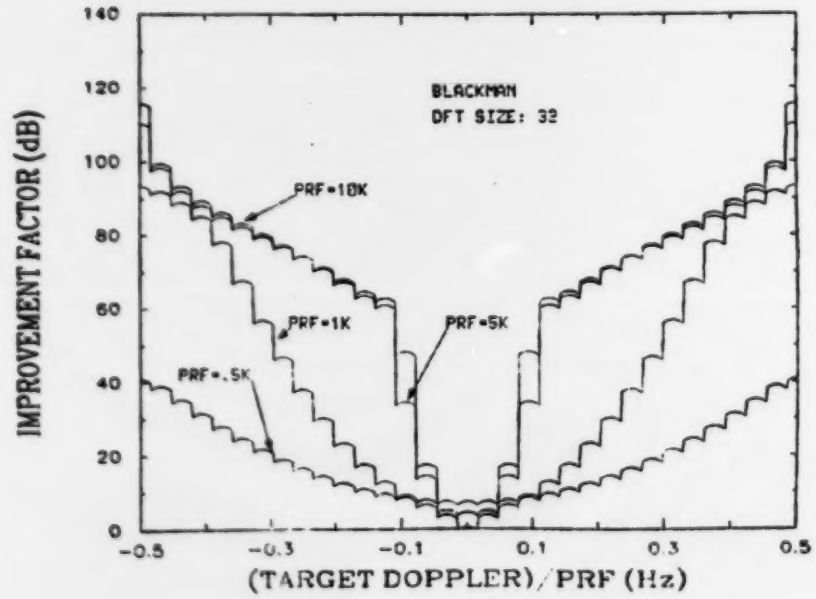

Figure 7: The Effect of the PRF (block size fixed)

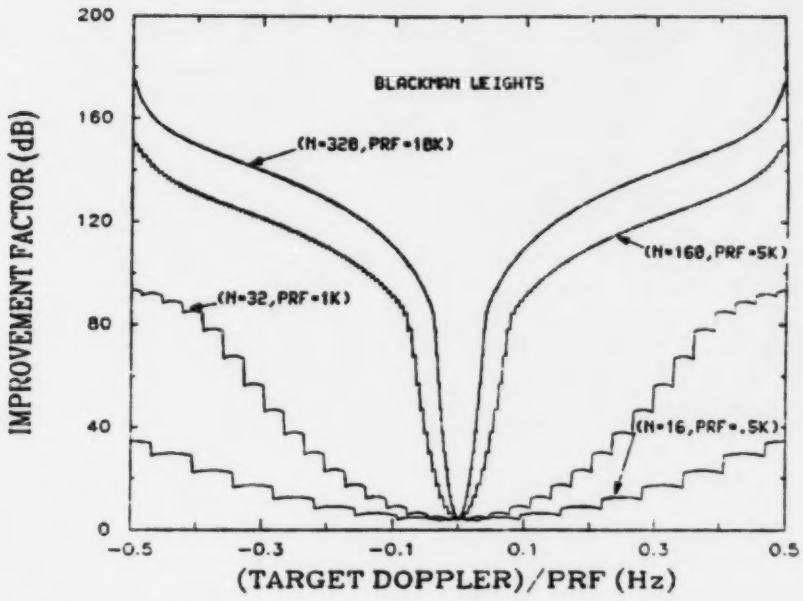

Figure 8
The Effect of the PRF (block size variable)

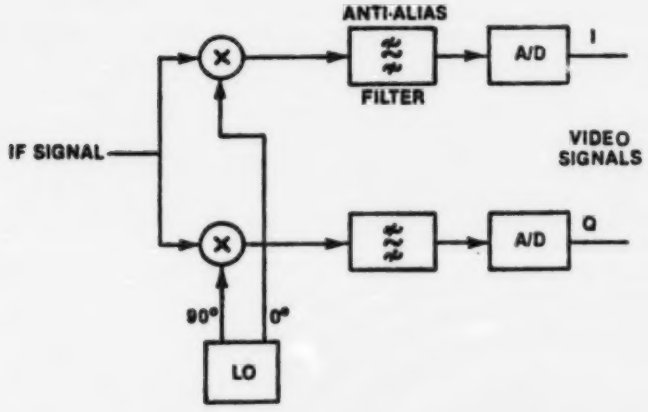

Figure 9
Quadrature Receiver

basis of fixed dwell time, the effect of increasing the PRF is to increase the block size. In terms of the example of the previous paragraph, we should compare a PRF of 1 kHz, block of 32 samples extending over 32 milliseconds, resolution of 1kHz/32 to a PRF of 5 kHz, block of 160 samples extending over 32 milliseconds, resolution 5 kHz/160 = 1 kHz/32. Such a comparison is illustrated in Fig.8 where the advantages of increasing the PRF are much more evident than in Fig 7. As Fig.8 shows, an increase in PRF leads to an increase in the Doppler visibility region.

3.2 CORRECTION OF SYSTEMATIC ERRORS

Another important task performed by the MDPU is the correction of systematic errors. A novel approach is proposed for the correction of multiple channels. We first correct for quadrature errors in the I and Q receivers for each channel and then correct for the phase and amplitude imbalances between each of the eight receiver channels of the eight–element vertical array.

It is essential to first correct for I and Q orthogonality within each channel before correcting for phase and amplitude differences between channels; phase errors between channels cannot be measured accurately unless the I and Q receiver channels are orthogonal.

3.2.1 CORRECTION OF I AND Q IMBALANCES

An important source of errors are the imbalances, in gain and phase, of the I and Q channels. These, if not corrected, can lead to a mismatch between the model used in the CHA and the actual measured data, causing errors in the estimated target height. Errors in the I and Q channels must be corrected in order to achieve sufficient accuracy for the CHA algorithm.

This section presents a method [19] for correcting the I and Q errors by means of correction coefficients which are derived from measurements of a test signal. The form of a quadrature reception is illustrated in Fig.9. The IF (intermediate frequency) input signal is decomposed into in–phase (I) and quadrature (Q) components and digitized before transfer to the MDPU. Under ideal conditions, the gain of the two channels are equal and the relative phase difference between channels is 90 degrees. Let

$$X(t) = I(t) + j\,Q(t) \tag{13}$$

where

$$I(t) = A \cos(\omega t + a) \tag{14}$$
$$Q(t) = A \sin(\omega t + a) \tag{15}$$

where a is the unknown phase and ω is the signal frequency (radians/second).

Because of unavoidable components differences, the frequency response of the two channels will be different causing a departure from orthogonality. This can be modelled by introducing phase and gain errors in the signal paths:

$$I(t) = A\,(1 + \epsilon) \cos(\omega t + a) + a \tag{16}$$
$$Q(t) = A \sin(\omega t + a + \phi) + b \tag{17}$$

where a and b are dc offset errors in the analog–to–digital, (A/D), converter, ϵ is a gain error and ϕ is a phase error.

The baseband signal Y(t) before A/D conversion is written as

$$Y(t) = \frac{(1+\epsilon)\ A}{2}\left[e^{j(\omega t+a)} + e^{-j(\omega t+a)} \right] + a$$
$$+ j\,(A/2)\left[e^{j(\omega t+a+\phi)} - e^{-j(\omega t+a+\phi)} \right] + jb \tag{18}$$

Equation 18 can be expressed in terms of X(t) as

$$Y(t) = [X(t)/2]\left[1 + \epsilon + e^{j\phi} \right]$$
$$+ [X^*(t)/2]\left[1 + \epsilon - e^{-j\phi} \right] + a + jb \tag{19}$$

Thus, one can see that I, Q gain and phase imbalances affect the output Y(t) by transferring a fraction

$$[1/2]\left[1 + \epsilon - e^{-j\phi} \right] \tag{20}$$

of the gain to the image $X^*(t)$ (opposite frequency) as well as adding a dc component

(a + jb). The magnitude of the image response relative to the input signal is given by

$$\mathrm{ISR} = 20 \log \left| \frac{1 + \epsilon - e^{j\phi}}{1 + \epsilon + e^{j\phi}} \right| \tag{21}$$

where ISR is the image to signal ratio.

From (19), one can see that the power output of the unbalanced signal appears at only three frequencies; the signal frequency, ω, the image frequency $-\omega$ and dc. I and Q errors can be corrected by means of correction coefficients which are derived from measurements of a test signal. The test signal is characterized by a high SNR, much higher than that of the real signal. The test signal can be injected at the IF stage.

Three digital filters are formed; one at dc, one at the test signal frequency and one at the image of the test signal frequency. Let (19) be written as

$$Y(t) = A(1+\epsilon) \cos(\omega t + a) + a + jA \sin(\omega t + a + \phi) + jb \tag{22}$$

If we evaluate the Fourier transform of Y(t), $F(\xi/\omega)$, at $\xi = 0, \omega, 2\omega$, and 3ω, we obtain

$$F(0) = a + jb \tag{23}$$

$$F(1) = (A/2)(1 + \epsilon + \cos\phi + j \sin\phi)\, e^{ja} \tag{24}$$

$$F(2) = 0 \tag{25}$$

$$F(3) = (A/2)(1 + \epsilon - \cos\phi + j \sin\phi)\, e^{-ja} \tag{26}$$

The use of a four–point DFT at frequency ω will provide the desired values of F(0) to F(3).

The correction coefficients are obtained from the ratio [19].

$$\frac{2\ F(3)}{[F^*(1)\ + F(3)]} = 1 - \frac{\cos\ \phi}{1 + \epsilon} + j \frac{\sin\ \phi}{1 + \epsilon} \tag{27}$$

Fig. 10 shows a block diagram for the correction of the I and Q errors in a single channel based on (27). We simultaneously apply the correction on all the channels based on (27) as follows:

$$\begin{bmatrix} I_{ic} \\ Q_{ic} \end{bmatrix} = \begin{bmatrix} E_i & 0 \\ P_i & 1 \end{bmatrix} \begin{bmatrix} I_{iu} \\ Q_{iu} \end{bmatrix} \tag{28}$$

where i is the channel subscript, I and Q indicate quadrature channel outputs and c and u indicate corrected or uncorrected. The correction coefficients for the i^{th} channel, E_i and P_i, are given as

$$E_i = \frac{\cos \phi_i}{1 + \epsilon_i} \tag{29}$$

$$P_i = -\frac{\sin \phi_i}{1 + \epsilon_i} \tag{30}$$

3.2.2 MULTICHANNEL METHOD

A new method is proposed to correct the amplitude and phase differences between channels in a multichannel receiving systems such as the ELAT system. The correction method described in the previous section is expanded to a multichannel environment in order to equalize all channels.

First of all, the correction for orthogonality is performed for each channel using a test signal which is applied to all channels simultaneously. After correction, the I and Q channels can be represented by the following set of equations where all the I and Q channels are orthogonal but there are differences in amplitude and phase between channels. The I and Q outputs of the i^{th} channel are represented as

$$I_i = A_i \cos(\omega t + a_i) \tag{31}$$

$$Q_i = A_i \sin(\omega t + a_i) \tag{32}$$

where i=1,2,...,M and M is the number of antenna channels; a_i is the arbitrary phase of the i^{th} channel; A_i is the arbitrary amplitude of the i^{th} channel.

It is now possible to correct the phase and amplitude differences, a_i and A_i, between channels by a process similar to that used to correct the individual channels. We first illustrate the technique for two channels and we then show how to extend it to any number of channels.

We start with the equations for the I and Q outputs of channels one and two, as follows:

$$I_1 = A_1 \cos(\omega t + a_1) \tag{33}$$
$$Q_1 = A_1 \sin(\omega t + a_1) \tag{34}$$
$$I_2 = A_2 \cos(\omega t + a_2) \tag{35}$$
$$Q_2 = A_2 \sin(\omega t + a_2) \tag{36}$$

Equations 33–36 can be rearranged and written in the same form as 16–17 as

$$I_1 = B(1 + g_{12}) \cos(\omega t + a_1) \tag{37}$$
$$Q_2 = B \sin(\omega t + a_1 + \theta_{12}) \tag{38}$$
$$I_2 = B \cos(\omega t + a_1 + \theta_{12}) \tag{39}$$
$$Q_1 = B(1 + g_{12}) \sin(\omega t + a_1) \tag{40}$$

where g_{12} and θ_{12} are respectively the gain error and the phase error between channel 1 and channel 2. We observe that $B(1+g_{12}) = A_1$ and $B = A_2$.

The correction to make I_1 and Q_2 orthogonal is derived directly from (28–30):

$$\begin{bmatrix} I_1' \\ Q_2' \end{bmatrix} = \begin{bmatrix} E_{12} & 0 \\ P_{12} & 1 \end{bmatrix} \begin{bmatrix} I_1 \\ Q_2 \end{bmatrix} \tag{41}$$

Requiring that the four components must be equal, we find that the correction to apply to $[I_2, Q_1]$ is

$$\begin{bmatrix} I_2' \\ Q_1' \end{bmatrix} = \begin{bmatrix} 1 & -P_{12} \\ 0 & E_{12} \end{bmatrix} \begin{bmatrix} I_2 \\ Q_1 \end{bmatrix} \tag{42}$$

with

$$E_{12} = \frac{\cos \theta_{12}}{1 + g_{12}} \tag{43}$$

$$P_{12} = -\frac{\sin \theta_{12}}{1 + g_{12}} \tag{44}$$

where g_{12} and θ_{12} are the gain and phase errors between channels 1 and 2. This transformation makes channel 1 identical to channel 2 with

$$I_1' = I_2' = B \cos \theta_{12} \cos (\omega t + a_1) \tag{45}$$

$$Q_1' = Q_2' = B \cos \theta_{12} \sin (\omega t + a_1) \tag{46}$$

A third channel can be corrected with respect to either channel 1 or channel 2. Fig 11 shows a scheme where channel 3 is corrected with respect to channel 2 , followed by a correction of channel 4 with respect to 3. When channel 3 is compensated with respect to 2, the amplitude of 2 is changed by a factor E_{23}. Therefore the balance with 1 is upset. This is compensated by multiplying channel 1 outputs by the factor E_{23}. A similar upset occurs when channel 4 is compensated with respect to channel 3. Therefore, channel 1 is multiplied by the product, $E_{12}\ E_{23}\ E_{34}$, channel 2 by the product $E_{23}\ E_{34}$ and channel 3 by E_{34} as in Fig.11. The extension of the scheme to any number of channels is evident. The compensation coefficients, $E_{12}\ E_{23}\ E_{34}$, and $E_{23}\ E_{34}$ can applied as products rather than as shown in Fig.11 where they are applied individually. This will reduce the number of multiplications, so that the number of operations is the same for each channel. We recommend correcting each channel with respect to a selected reference channel to avoid accumulation of errors with finite arithmetic.

This method has the potential to correct not only the I and Q imbalances but also the misalignment of the vertical antenna array which can be represented by phase and amplitude differences between antenna channels. In this case, we require a programmable Doppler–signal calibration facility producing an RF (radio frequency) test signal for illuminating the antenna elements of the vertical feed array. This facility is being developed for the ELAT radar receiver system.

3.2.3 I AND Q CORRECTION IN THE DOPPLER FREQUENCY DOMAIN

We correct only the Doppler filter output corresponding to the target velocity to obtain a large reduction in the computation load. Doppler filtering is implemented by means of an N–point transform applied to appropriately windowed data coming from each of eight antenna receiver channels and corresponding to the selected target range cell. In total, eight N–point transforms are formed. The target range cell has been previously determined using the TART processor which does the initial target detection.

We find the Doppler bin corresponding to the target by 1) summing the amplitudes for each Doppler bin across the eight antenna outputs to give N integrated Doppler–bin outputs and 2) choosing the largest integrated Doppler–bin output to indicate the target Doppler bin.

The uncorrected output of the m^{th} filter in the i^{th} channel, (i=1 to 8), is given by

$$F_i(1) = (A_i/2)\,(1 + \epsilon_i + \cos\phi_i + j\sin\phi_i)\,e^{j\alpha_i} \tag{47}$$

where $F_i(\xi/\omega)$ is the Fourier transform of the target signal with Doppler velocity ω as received on the i^{th} antenna channel.

The desired signal after correction for I and Q orthogonality errors is

$$F_i'(1) = (A_i/2)\,e^{j\alpha_i} \tag{48}$$

The correction coefficients, ϵ_i and ϕ_i, are pre–determined using the method described in section 3.2.1. We use a test signal with power very much larger than the receiver noise power to determine the following quantities for i=1 to 8:

$$COEF_i = 1 - \frac{\cos\ \phi_i}{1 + \epsilon_i} + j\frac{\sin\ \phi_i}{1 + \epsilon_i} \tag{49}$$

To correct the signal in the frequency domain, we first solve for ϵ_i and ϕ_i using (49) and then determine the correction coefficient for I and Q errors as:

$$COEF'_i = (1 + \epsilon_i + \cos \phi_i + j \sin \phi_i) \quad (50)$$

We correct for I and Q errors using (50) by forming

$$F_i'(1) = F_i(1)/COEF'_i \quad (51)$$

for each of i=1 to 8 channels. It is then necessary to balance the channels by correcting for the residual phase and amplitude errors, ϕ_i and A_i. This is done during tracking using the multichannel technique of section 3.2.2 (illustrated in Fig.11).

3.2.4 ESTIMATION OF THE CORRECTION COEFFICIENTS USING A PROTOTYPE–QUADRATURE RECEIVER

We carried out an experiment to verify the method for correcting for I and Q imbalances using a real quadrature receiver. The experimental setup is shown in Fig.12. The input test signal is generated using a single sideband generator. The system under test consists of a balanced modulator followed by two anti–aliasing filters (0–5)KHz and two A/D converters. A fast memory is provided via the Kontron emulator and the data are transferred to a VAX 780 using Kermit software and an IBM–PC. Analysis of the data is carried out on the VAX 780.

After frequency down–conversion and low–pass filtering, the test signal at the input to the A/D converters occupies a band (0–5kHz). The 5 KHz upper limit is set by the anti–aliasing filters. We note here that a performance study of the general correction process in which noise and multiple channels are considered is beyond the scope of this report. However this simple experiment provides verification of the basic I–Q correction technique which is the basis of the multichannel calibration technique. Further studies will be undertaken to analyze the correction process over a wider Doppler frequency band and using the ELAT multiple channel receiver when the design of the latter is finished.

Nevertheless, the application of the correction method over the (0–5)kHz Doppler band gives very good results. A FFT is applied to the data and the coefficients are derived according to the process described in the previous section. Examples of results are presented in Figs 13 and 14 where the dc and the image level are at –30 dB and –35 dB respectively. The image and dc are corrected with the same set of coefficients and the final

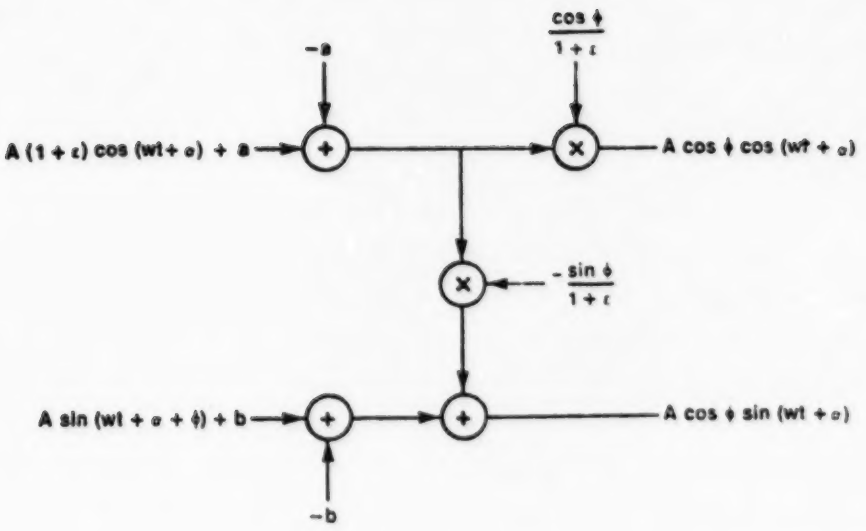

Figure 10
Correction of I and Q Imbalances

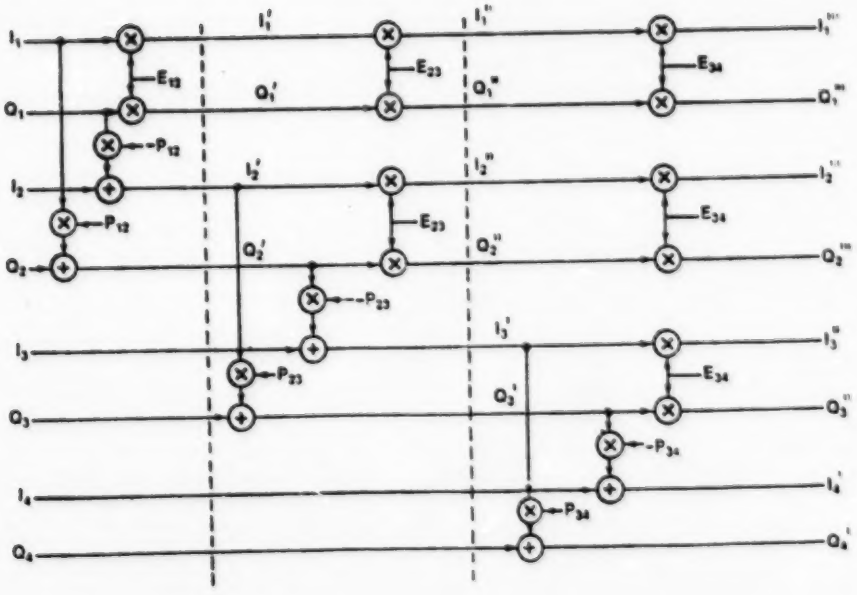

Figure 11
Multichannel Correction Process

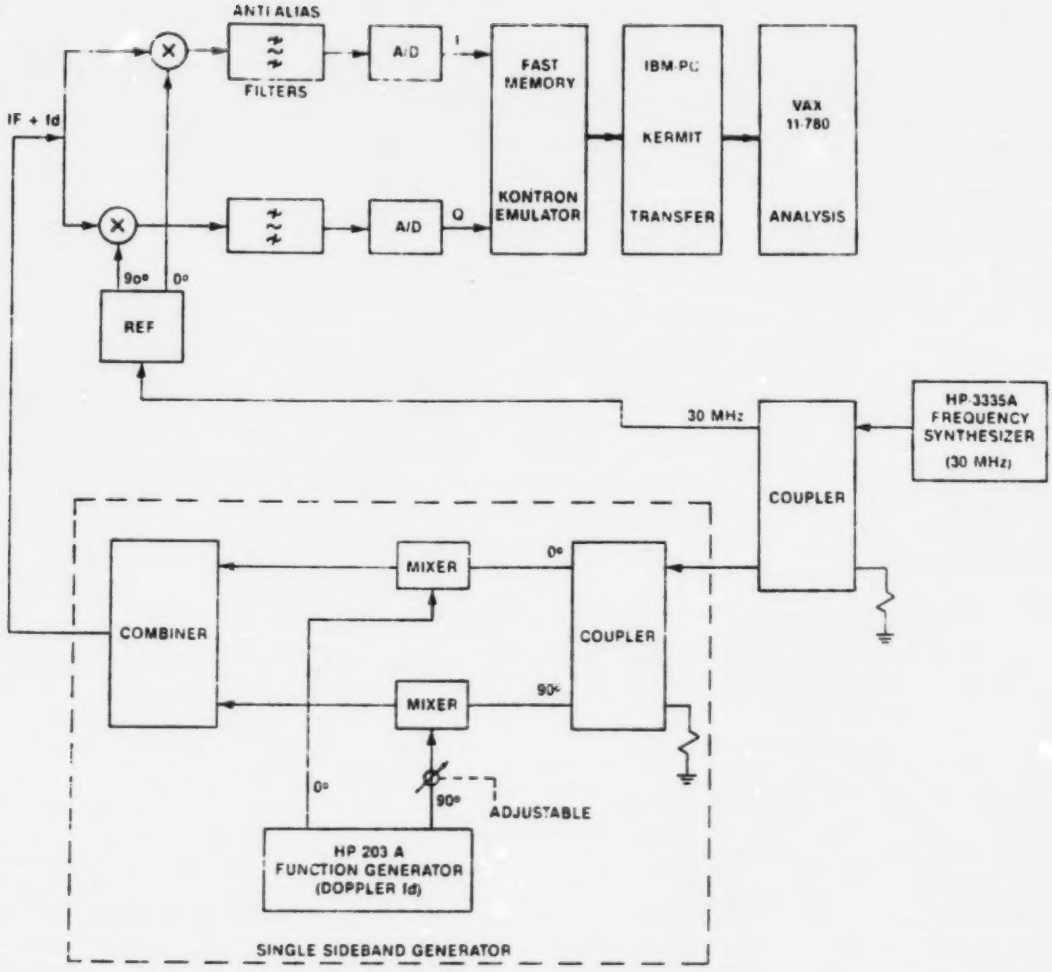

Figure 12
Experimental Setup to Estimate the Correction Coefficients

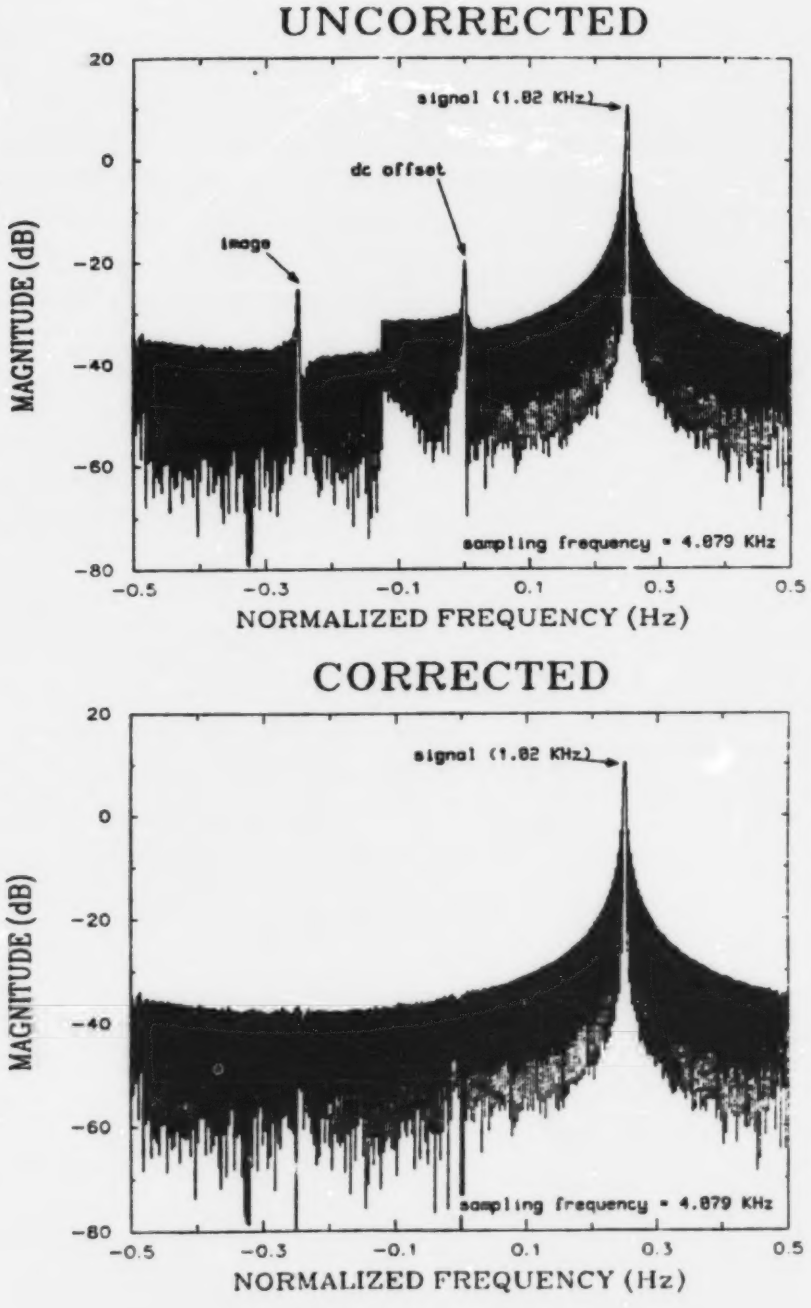

Figure 13

Example of Correction of I and Q for Doppler Frequency of 1.02 KHz

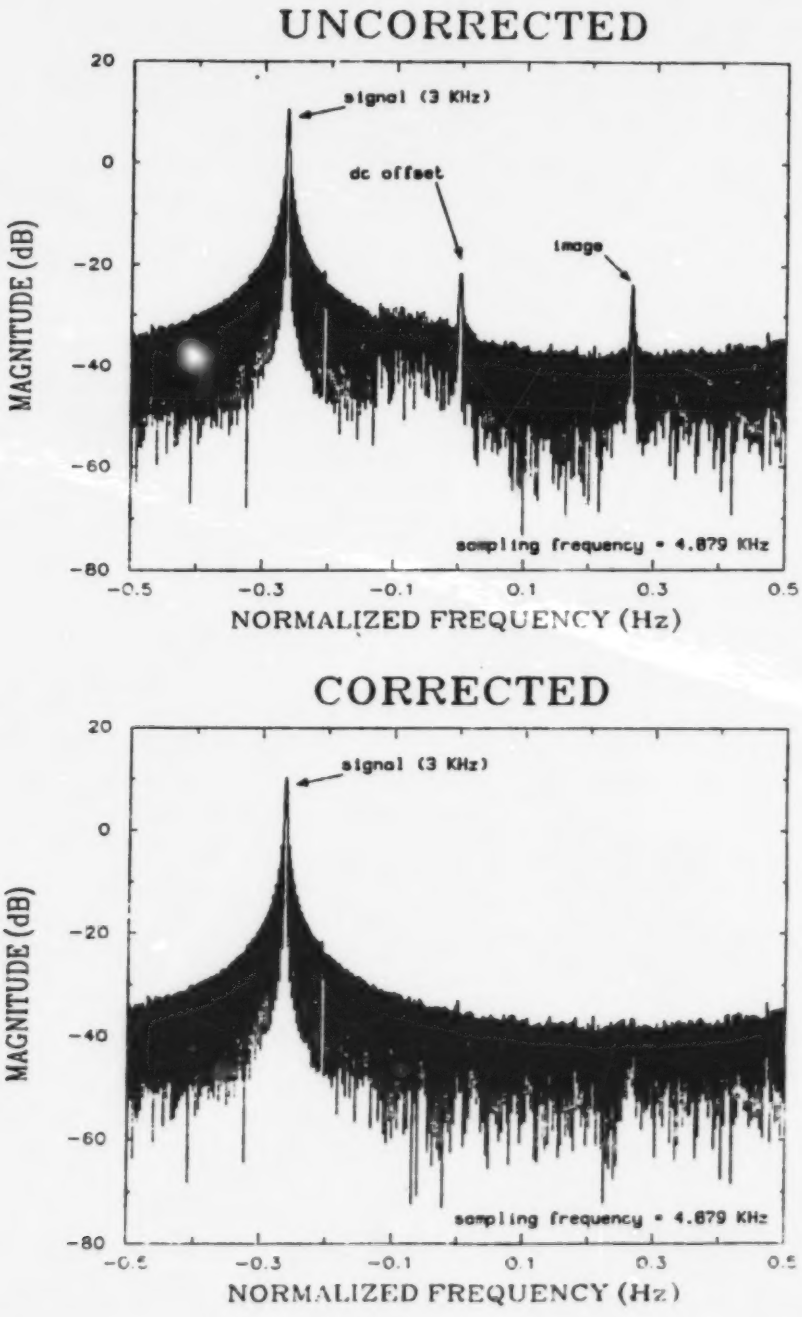

Figure 14

Example of Correction of I and Q for a Doppler Frequency of 3 KHz
(using same correction coefficients than in fig.13)

results show a sidelobe structure completely restored. The test has been repeated over the complete simulated Doppler band (0–5)kHz using the same set of correction coefficients (independent of the frequency) and giving results similar to those in Figs 13 and 14. Further experiments should be conducted to analyze the correction process over a more extended Doppler band.

4.0 REAL–TIME IMPLEMENTATION OF THE MDPU:

In this section, we establish the real–time requirements of the MDPU and propose an implementation using a commercial array processor.

4.1 REAL–TIME PROCESSING BUDGET:

The easiest way to study the real–time requirements of the MDPU is to divide the system into major subsystems and examine these individually. Figure 15 shows the MDPU block diagram. Each block corresponds to a specific function and will be studied with regard to its real–time requirements. The MDPU functions are

1) Weighting
2) DFT (Doppler processing)
3) Detection: form magnitude and select largest
4) Amplitude and phase correction for I and Q imbalances
5) Correction for misalignment of the vertical array.

In the development of the time budget for these operations, we start with the upper limit to the input data rate to the CHA processor. This processor can function at a maximum rate of 50 Hz [16]; it can thus accept and analyze one integrated data vector from the antenna array every 20 milliseconds. The ELAT system is designed to work with two independent magnetron transmitters, each transmitting at a maximum PRF of 1000 Hz with interlaced pulse trains at RF frequencies, f_1 and f_2. In order to keep up with the real–time capability of the CHA processor, we have to deliver to the latter, two processed blocks of length n_b, one for frequency f_1 and the other for f_2, every 40 milliseconds. These blocks must be processed in the 40 milliseconds processing interval and collected in the 40 milliseconds prior to the processing interval. This procedure requires two memory blocks,each of length 2 n_b with

$$n_b = 40 \times 10^{-3} \text{ PRF} \quad (52)$$

For PRF = 1000 Hz we get $n_b = 40$. That is, the Fourier transform block size must be of length 40 or longer. We assume a standard "ping–pong" memory system where one block is being filled while the other is being processed. The operations listed above must be carried out for two frequencies. Therefore a data block of length n_b must be completely processed every 20 milliseconds in order to maintain real–time operation.

4.1.1 WEIGHTING

The weighting process is performed using two real multiplications for each complex sample. (Samples are complex but weights are real.) There are 2 n_b x 8 antenna channels for a total of 16 n_b real multiplications per processing interval.

4.1.2 FFT IMPLEMENTATION

We have to perform an FFT for each of two frequencies and eight antenna channels for a total of 16 FFT's. The block length is made equal to 64, the smallest power of two greater than the minimum block length of 40. We therefore must carry out 16 64–point FFT's every 64 milliseconds in addition to all of the other operations listed previously. A board–level array processor, the Mercury ZIP 3232 [20] can perform 16 64–point FFT's in 3.44 milliseconds. This is more than adequate for our requirements.

4.1.3 DETECTION: FORM MAGNITUDE AND DETECT LARGEST

The objective is to determine the complex vector to be sent to the CHA data processor via the distribution network (Fig.1). The magnitude of each complex DFT output is found and these are summed across the M channels. The maximum value determines which is the target Doppler bin and hence, which filter output to use as the desired complex vector (M complex samples). Forming the magnitude requires two real multiplications, one square root and one addition for each FFT output (N) and for each antenna element (M). To sum across the M channels we need N(M–1) additions. Finally N comparisons are required to determine the largest.

4.1.4 AMPLITUDE AND PHASE CORRECTION FOR I AND Q IMBALANCES

Since the detection algorithm allows the determination of the complex vector corresponding to the target Doppler frequency, the amplitude and phase correction need only to be applied to this complex vector. The amplitude and phase correction process shown in Fig.11 requires only three additions and two multiplications for each complex channel.

4.1.5 CORRECTION FOR THE MISALIGNMENT OF THE VERTICAL ARRAY

The multichannel correction approach described in section 3.2.2 needs four real multiplications and two real additions to balance two adjacent channels. To balance M channels it requires 4(M–1) multiplications and 2(M–1) additions.

4.1.6 REAL–TIME BUDGET SUMMARY

The time budget for carrying out all of the above processing on a ZIP 3232 processor, assuming a block size of 64 samples for each of two RF frequencies, is as follows:

Weighting operations	1.16 ms
16.... 64–point FFT's	3.44 ms
Formation of magnitudes and detection	2.27 ms
Correction for channel errors	0.16 ms
Formatting	11.56 ms
Total.....	18.59 ms

Here formatting includes conversion to floating point, sorting, scaling and inverting where necessary. As the available time is 64 ms, the above implementation has a comfortable margin.

4.2 PROPOSED IMPLEMENTATION

The previous time budget indicates that all of the required operations can be implemented on the Mercury ZIP 3232 array processor with a comfortable performance margin. In fact the use of a larger block size, say 128 points may be supportable although a detailed analysis has not been done. Still another possibility is the use of additional RF frequencies. The ZIP processor could handle an additional four data blocks of length 64 in the 64–millisecond interval; this would allow for four additional frequencies. Board–level array processors of this type are highly suitable because of their programmable nature and reasonable cost. The ZIP 3232 from Mercury Systems [20] is attractive because of its speed and its 32–bit floating point architecture (Q–Bus). According to the specifications a 16 MFLOPS rate is possible. (ZIP performs a 1024–point complex FFT in 2.8 msec). SKY WARRIOR (15 MFLOPS) from SKY Computers is a possible alternative.

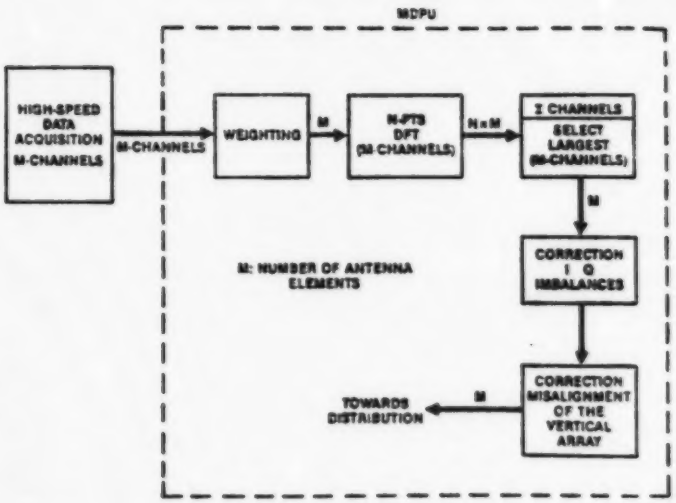

Figure 15: MDPU Functional Block Diagram

5.0 SAMPLING AND DOPPLER AMBIGUITIES IN ELAT

In this section, we describe the sampling in the ELAT system and derive the signal–to–noise ratios for both detection and estimation. We also consider the effects of velocity ambiguities and show how the PRF affects the Doppler visibility. We discuss the particular requirements of the ELAT system for clutter–free samples for estimation at both RF frequencies and suggest a method for controlling the PRF's to achieve this result.

The number of data samples available for coherent integration is dependent on the target speed, v, the radar range cell extent, ΔR, the time interval between data samples, T, and the position of the target in the range cell at the start of sampling, Δr. If the target takes a time interval, NT, to cross the range cell, then the maximum number of available signal samples is N. We cannot hope to synchronize the sampling to start at the instant the target crosses the range–cell boundary. Therefore, the actual number of signal samples taken in a block of data of fixed length will generally be less than N.

5.1 SAMPLING IN THE ELAT SYSTEM

The ELAT system uses two parallel data–acquisition systems to perform the detection and the target–height estimation (Fig.1). We use two 8–bit ADC's for the detection and multiple 12–bit ADC's for the estimation. We require the collection of two blocks of data. We use the first, of length N_d, to detect the target and designate the target range cell. The second, of length N_e, is sampled from the designated range cell and used for the CHA or ML height estimation. We define a block of data as being the collection of snapshots. The set of sensor outputs collected at a particular instant of time constitutes a snapshot.

The detection is carried out at the output of a moving–window FIR filter. The detection block is then a moving block. Every transmit pulse a new sample enters the block and the oldest is ejected. At each pulse repetition interval (PRI) a target is declared in the range cell which provides the maximum coherently–integrated output. Then the data–acquisition system for the estimation block samples the designated range cell one PRI later.

The estimation of target height is a fixed–window process. The N_e data samples used for estimation are taken from the designated target cell, coherently integrated, and

passed to the CHA processor for target–height estimation. The target is moving, and the estimation block may be filled or partially filled with useful signal samples. The number of useful signal samples depends on the position of the target in the range cell at the start of sampling as well as the target speed, the inter–pulse interval and the size of the data blocks, N_d and N_e. If the target crosses from one range cell to another when an estimation block is being sampled, the TART unit indicates a change of range cell.

We designate Δr as the position of the target in the range cell A at the start of the sampling of the detection block. If we consider an ensemble of random starting positions, then Δr is uniformly distributed in the range $0 < \Delta r < \Delta R$. We designate the number of useful signal samples from cell A or cell B in the detection and estimation blocks as $n_d(A)$ or $n_d(B)$ and $n_e(A)$ or $n_e(B)$ respectively. These are random variables that depend on Δr as shown in Fig.16 with Δr measured to the left and with a target moving from right to left. Here we consider only the case where $N_d \leq N$. When $N_d > N$, the number of useful signal samples is fixed at N, while the number of noise–only samples is $N_d - N$. Therefore as N_d increases beyond N, the signal–to–noise ratio decreases because of the increasing number of noise–only samples. In Fig.16, we assume that all events occur without delay.

In Fig.16, we observe that $n_d(A)$ starts decreasing when no time is left to collect N_d samples in range cell A. By that time, $n_d(B)$ starts to increase to attain the detection threshold and the target is declared in range cell B. The greatest of $n_d(A)$ and $n_d(B)$ constitutes the number of useful signal samples n_d for the detection block.

The estimation block starts to sample after $N_d/2$ samples have been collected in the detection block (i.e. $n_d(A,B) = N_d/2$) and the target range cell has been detected. However, the target may leave range cell A before the estimation block has been filled as indicated by the decreasing value (going to the left) of $n_e(A)$ as a function of Δr. We designate $n_e(B)$ as the number of estimation samples that would be collected if the sampling was, instead, carried out in range cell B immediately to the left of range cell A. $n_e(B)$ starts to increase from zero where $n_e(A)$ starts to decrease.

The TART unit indicates the range cell where the target lies in and gives a change–of–range–cell indication when the count $n_d(B) > N_d/2$. Since the TART is a moving–window integrator, the change–of–range–cell indication is given late, $N_d/2$ pulses

after the target has left range cell A. This means that at most $N_d/2$ samples from the estimation block can be taken from the wrong range cell before a change–of–range–cell indication occurs. However, if we switch range cells for the estimation block while the block is being formed, we obtain a mixture of clutter–plus–noise samples from cell A and cell B. Consequently, signals from the two cells will not add coherently resulting in a signal loss. Much more important, however, is the loss in coherence for the clutter block which prevents the filters from rejecting clutter properly. For this reason, we continue sampling the estimation block in the range cell when the sampling was started until the block is full. This causes some additional signal loss associated with the bottom curve of Fig.16 but the clutter block is coherent and will be properly filtered and rejected.

Sample block sizes of $N_d = N_e = 64$ samples have been chosen for ELAT as providing an acceptable integration gain, acceptable degree of clutter rejection and a reasonable degree of data reduction. The latter is required so that the CHA algorithm can cope with the real–time processing load. Note that N_d can be different from N_e.

The ELAT radar has three proposed modes of operation: mode 1 with a PRF of 1000 Hz and a pulse width of 0.2 microseconds, mode 2 with a PRF of 1000 Hz and a pulse width of 0.5 microseconds and mode 3 with a PRF of 500 Hz and a pulse width of 1 microsecond.

The performance criterion applied to these operational modes is that the N_e block be completely filled, 80% of the time. With reference to Fig.16, we calculate that

$$.80 = [N - N_e]/N \tag{53}$$

Substituting $N_e = N_d = 64$, we obtain $N = 320$ pulse intervals required by the target to fly a distance ΔR. For this value of N we calculate the limiting velocities for mode 1, 2, and 3 as Mach 0.287, Mach 0.71 and Mach 0.71, respectively using the expression

$$v_{max} = \Delta R/NT = \Delta R\ PRF/N \tag{54}$$

5.2 SIGNAL–TO–NOISE RATIO ANALYSIS

The signal–to–noise ratios are functions of $E(n_d^2)$ and $E(n_e^2)$. These can be obtained by averaging n_d^2 and n_e^2 over an interval of length ΔR in Fig.16. This is equivalent to assuming that Δr varies uniformly over an ensemble of random starting positions.The SNR's are designated as SNR_d for the detection and SNR_e for the estimation block of data. The SNR's are defined as

$$SNR_d = G\, E(n_d^2)/ (2\, \sigma^2\, N_d) \tag{55}$$

$$SNR_e = E(n_e^2)/ (2\, \sigma^2\, N_e) \tag{56}$$

where E( ) indicates the statistical expectation, σ^2 is the noise power on a single antenna array–element receiver and G indicates the beamforming gain obtained by combining all the vertical–array element outputs in a beamforming network in the ELAT radar. For simplicity, we will set G = 1 in what follows. Actual values for SNR_d may then be obtained by increasing the results by the beamforming gain.

We average n_d^2 and n_e^2 over an ensemble of random starting locations, Δr. An equivalent result is obtained by averaging over an interval of length, ΔR. To illustrate the method, consider the diagram for the variation of n_d in Fig.16. Here we see that $n_d = N_d$ for a fraction of a range cell, $(N–N_d)/N$, and n_d is uniformly distributed between $(N_d)/2$ and N_d for a fraction, $(N_d)/N$. Therefore,

$$E(n_d^2) = N_d^2\,(N–N_d)/N + [(N_d)/N]\,[2/(N_d)] \int_{N_d/2}^{N_d} n_d^2\, dn_d \tag{57}$$

After some manipulation, we obtain

$$SNR_d \approx \frac{G}{2\ \sigma^2}\left(N_d - \frac{5\ N_d^{\,2}}{12\ N}\right) \tag{58}$$

We use the same methodology as above to find SNR_e. We see that $n_e = N_e$ for a fraction of a range cell, $[N - N_e)]/ N$; n_e is uniformly distributed between 0 and N_e for a fraction, N_e/N . Evaluating $E(n_e^2)$ for this distribution, and substituting into the expression for SNR_e gives

$$SNR_e \approx \frac{1}{2\sigma^2}\left(N_e - \frac{2N_e^2}{3N}\right) \qquad (59)$$

5.2 VELOCITY AMBIGUITIES

The coherent integration applied to both the N_d and N_e data blocks is a type of digital filtering which is affected by aliasing when the sampling frequency is "too low". These aliasing effects are present in the ELAT radar since the transmitter will not allow the use of a sufficiently high PRF to give unambiguous filter responses for the entire range of target velocities of interest.

5.2.1 DOPPLER VISIBILITY REGION

The ELAT radar operates at two RF frequencies, f_1 = 9.6 GHz and f_2 = 8.6 GHz, and has two PRF's corresponding to modes 1 and 2 (PRF = 1000 Hz) and mode 3 (PRF = 500 Hz). Since the height–estimation algorithms require clutter–free samples at both frequencies, simultaneously, the requirement for a clutter–free Doppler visibility region is more severe than for detection. For modes 1,2, the aliased or blind velocities are v_{b1} = 30.372 knots and 33.92 knots corresponding to RF frequencies, f_1 and f_2. For mode 3, the ambiguities occur at v_{b1} = 15.186 knots and v_{b2} = 16.96 knots. The sea clutter, with a spectrum concentrated at low velocities, will also be aliased and it will not be possible to detect targets having velocities lying within the aliased clutter spectra. The clutter Doppler spread for sea state 3 can be estimated from Fig.6 as 340 Hz for a block size of 32, a Blackman filter window and a 1 m^2 target cross section. This is 10.32 knots at 9.6 GHz. Since the two RF's are different there will be times when the cluttered regions nearly fully overlap and other times when they are contiguous. An average situation might be when they are half overlapped which gives a clutter blocked region of about 15 knots out of an available 30 knots. From these considerations, one can see that the use of such a low PRF for ELAT severely constrains its operations. Given uncertainties about the velocity of the ship as well, the difficulty of putting even a cooperative target in a clear window is severe. For these reasons, it appears best to rely on super clutter visibility using a large target.

5.2.2 PRF AGILITY

The present ELAT radar is designed as a demonstration system to work with cooperative targets. The close spacing of the velocity ambiguities is undesirable for an operational system. An increase of the PRF to the region of 5–10 kHz is very desirable for a future system. The first range ambiguity occurs at 15 Km for the 10 KHz PRF and at 30 km for the 5 KHz PRF. For target tracking within these limits, range ambiguities should not pose any problems. There will, however, be velocity ambiguities. For the 10 KHz PRF, the velocity ambiguities for the two RF frequencies are 339.2 knots for 9.6 GHz and 303.7 knots for 8.6 GHz. The corresponding values for 5 KHz are 169.9 and 151.9 knots. Since target velocities are expected to be higher than Mach 1, velocity ambiguities and blind velocities will occur. These must be resolved by changing the PRF. In generating the PRF changes, it is important to realize that clutter–free samples must be obtained at both RF frequencies. Therefore it is desirable to force the ambiguities at the two RF frequencies to coincide. This can be done by making $PRF(f_1)/PRF(f_2) = f_1/f_2$, where f_1 and f_2 are the two RF frequencies. If several RF frequencies are used, than $PRF(f_1)/PRF(f_n) = f_1/f_n$. Velocity ambiguities are then resolved by changing $PRF(f_1)$ by an amount, DF, and $PRF(f_n)$ by an amount $DF[f_1/f_n]$.

6.0 CONCLUSION

This report analyses the requirements of the high–speed MDPU Doppler–processing unit for improved SNR, reduced data rate, rejection of clutter and effective array and receiver calibration procedures. As a result of this analysis, a design for the MDPU is proposed based on the use of the Fast Fourier Transform (FFT) with a Blackman window. It is shown that this design can be realized as a programmable signal processor by using a commercially available array processor system. A new system for calibration of the array and the receiver phase and amplitude errors is described. The validity of this technique was verified experimentally. In addition, we give an original analysis of the effects of block processing on both the signal–to–noise ratios and the probability of obtaining specified numbers of missing signal samples as a result of target motion.

7.0 ACKNOWLEDGEMENTS

The authors thank Dr. Denis Faubert for reviewing this report.

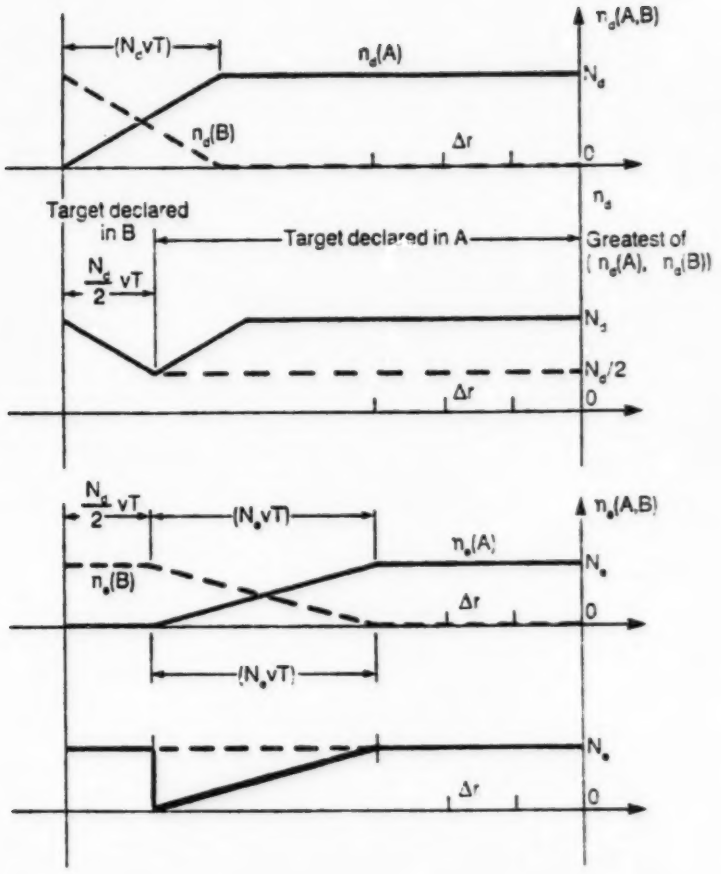

Fig.16 : The effects of target motion on sampling

8.0 REFERENCES

1. Rook, B.J., Litva, J., "An Improved CHA Algorithm For Tracking Low Angle Targets", CRC Report No.1356, Ottawa, 1982.

2. Bossé, É., Turner, R., " Height Ambiguities in Maximum Likelihood Estimation with a Multipath Propagation Model ", 22nd Asilomar Conference on Signals, Systems and Computers , Pacific Grove, CA, Oct.31–Nov.2, 1988.

3. Turner, R., Bossé, É., " The Use of Highly Refined Propagation Models in Maximum Likelihood Estimation of Target Elevation for Radar Tracking of Low–Altitude Targets Over the Sea ", EUPSICO–88, Sept.5–8, Grenoble, France, 1988.

4. Turner, R., Bossé, É., " Maximum Likelihood Tracking Using a Highly Refined Multipath Model ",21st Asilomar Conference on Signals, Systems and Computers , Pacific Grove, CA, Nov.2–4, 1987.

5. Bossé, É., Caseault, J., Fines, N.R., " A Description of the ELAT Distributed Computing System ", CRC Report No.1425, Ottawa, 1987.

6. DaSylva, P., Menard, P., Roy, D., " Development of a Programmable Finite Impulse Response Filter for Sea Clutter Rejection ", Final Report, Interactive Circuits and Systems Ltd, Ottawa, March 1986.

7. Norris, A.P., Wong, A.C., Pearson, A., Allsop, B.E., " CRC Radar Front–End Study ", Final Technical Report, Contract NO UK–83–0331/1, STL LTD, London, 1984.

8. Strickland, P., Wight, J., Jempson, A., " Experimental Low Angle Tracking Radar (ELAT) Transmitter Stability Analysis ", Contract DREO–97714–05– 2908, Canadian Astronautics Ltd., Ottawa, Nov. 1985.

9. Schleher, D.C., ed., " MTI Radar ", Artech House, WA.,1978.

10. Nathanson, F.E., " Radar Design Principles: Signal Processing and the Environment ", N.Y., McGraw–Hill Co., 1969.

11. Meyer, D.P., Mayer, H.A., " Radar Target Detection ", AP, NY, 1973.

12. Berkowitz, R.S., " Modern Radar ", Wiley, New York, 1965, p. 480.

13. Barton, D.K., " Radar System Analysis " McGraw–Hill, New York, 1965, p.100.

14. Chan, H.C., " Multi–Frequency Measurement of Radar Sea Clutter at Low Grazing Angles ", CRC Report No. 1410, Ottawa, 1987.

15. Skolnik, M.I., " Radar Hanbook ", McGraw–Hill, New York, 1970.

16. Bossé, É., " Real–time implementation of the CHA algorithm on an Array Processor " , CRC Report No.1422, Ottawa, 1987.

17. Andrews, G.A., " Performance of Cascaded MTI and Coherent Integration Filters in a Clutter Environment ", NRL Report 7533, Mar.27, 1973.

18. Harris, F.J., " On the Use of Windows for Harmonic Analysis with the Discrete Fourier Transform ", Proc. IEEE, Vol. 66, No.1, Jan. 1978.

19. Churchill, F.E., Ogar, G.W., Thompson, B.J., " The Correction of I and Q Errors in a Coherent Processor ", IEEE Trans., Vol. AES–17, No.1, Jan. 1981, p.131.

20. Mercury Computer Systems Inc., "ZIP 3232 User's Manual"

DOCUMENT CONTROL DATA

(Security classification of title, body of abstract and indexing annotation must be entered when the overall document is classified)

1. ORIGINATOR (the name and address of the organization preparing the document. Organizations for whom the document was prepared, e.g. Establishment sponsoring a contractor's report, or tasking agency, are entered in section 8.)

DEFENCE RESEARCH ESTABLISHMENT OTTAWA
3701 CARLING AVE., NEPEAN, ONTARIO K1A 0Z4

2. SECURITY CLASSIFICATION (overall security classification of the document, including special warning terms if applicable)

UNCLASSIFIED

3. TITLE (the complete document title as indicated on the title page. Its classification should be indicated by the appropriate abbreviation (S,C,R or U) in parentheses after the title.)

MULTICHANNEL DOPPLER PROCESSING FOR AN EXPERIMENTAL LOW-ANGLE TRACKING SYSTEM (U)

4. AUTHORS (Last name, first name, middle initial)

É. BOSSÉ/R.M. TURNER

5. DATE OF PUBLICATION (month and year of publication of document)	6a. NO. OF PAGES (total containing information. Include Annexes, Appendices, etc.)	6b. NO. OF REFS (total cited in document)
MAY 1990	53	20

7. DESCRIPTIVE NOTES (the category of the document, e.g. technical report, technical note or memorandum. If appropriate, enter the type of report, e.g. interim, progress, summary, annual or final. Give the inclusive dates when a specific reporting period is covered.)

DREO TECHNICAL REPORT

8. SPONSORING ACTIVITY (the name of the department project office or laboratory sponsoring the research and development. Include the address.)

DEFENCE RESEARCH ESTABLISHMENT OTTAWA, OTTAWA, ONT. K1A 0Z4

9a. PROJECT OR GRANT NO. (if appropriate, the applicable research and development project or grant number under which the document was written. Please specify whether project or grant)	9b. CONTRACT NO. (if appropriate, the applicable number under which the document was written)
011LA15	

10a. ORIGINATOR'S DOCUMENT NUMBER (the official document number by which the document is identified by the originating activity. This number must be unique to this document.)	10b. OTHER DOCUMENT NOS. (Any other numbers which may be assigned this document either by the originator or by the sponsor)
DREO REPORT 1039	

11. DOCUMENT AVAILABILITY (any limitations on further dissemination of the document, other than those imposed by security classification)

- (X) Unlimited distribution
- ( ) Distribution limited to defence departments and defence contractors; further distribution only as approved
- ( ) Distribution limited to defence departments and Canadian defence contractors; further distribution only as approved
- ( ) Distribution limited to government departments and agencies; further distribution only as approved
- ( ) Distribution limited to defence departments; further distribution only as approved
- ( ) Other (please specify):

12. DOCUMENT ANNOUNCEMENT (any limitation to the bibliographic announcement of this document. This will normally correspond to the Document Availabilty (11). However, where further distribution (beyond the audience specified in 11) is possible, a wider announcement audience may be selected.)

13. ABSTRACT (a brief and factual summary of the document. It may also appear elsewhere in the body of the document itself. It is highly desirable that the abstract of classified documents be unclassified. Each paragraph of the abstract shall begin with an indication of the security classification of the information in the paragraph (unless the document itself is unclassified) represented as (S), (C), (R), or (U). It is not necessary to include here abstracts in both offical languages unless the text is bilingual).

In this report, we present an analysis of the performance requirements for a Multichannel Doppler Processing Unit (MDPU) which is part of the Experimental Low-Angle Tracking (ELAT) radar system. This doppler processing unit must perform the following functions: data reduction, signal-to-noise ratio improvement, sea-clutter rejection and correction for systematic errors. Before establishing the doppler processing requirements, we analyse the characteristics of the sea-clutter as a function of the ELAT radar parameters. Then, we present the general guidelines for the design of the MDPU, with emphasis on a new method to compensate for systematic errors. Finally, we consider the effects of block sampling on both target detection and target height estimation.

14. KEYWORDS, DESCRIPTORS or IDENTIFIERS (technically meaningful terms or short phrases that characterize a document and could be helpful in cataloguing the document. They should be selected so that no security classification is required. Identifiers, such as equipment model designation, trade name, military project code name, geographic location may also be included. If possible keywords should be selected from a published thesaurus. e.g. Thesaurus of Engineering and Scientific Terms (TEST) and that thesaurus-identified. If it is not possible to select indexing terms which are Unclassified, the classification of each should be indicated as with the title.)

Doppler Processing
Sampled Aperture
Digital Filtering